2017 IEEE International Conference on Robotics and Automation (ICRA)
Singapore, May 29 - June 3, 2017

RoboFDM: A Robotic System for Support-Free Fabrication using FDM

Chenming Wu[1*], Chengkai Dai[2*], Guoxin Fang[2], Yong-Jin Liu[1] and Charlie C.L. Wang[2†]

***Abstract*— This paper presents a robotic system – RoboFDM that targets at printing 3D models without support-structures, which is considered as the major restriction to the flexibility of 3D printing. The hardware of RoboFDM consists of a robotic arm providing 6-DOF motion to the platform of material accumulation and an extruder forming molten filaments of *polylactic acid* (PLA). The fabrication of 3D models in this system follows the principle of *fused decomposition modeling* (FDM). Different from conventional FDM, an input model fabricated by RoboFDM is printed along different directions at different places. A new algorithm is developed to decompose models into support-free parts that can be printed one by one in a collision-free sequence. The printing directions of all parts are also determined during the computation of model decomposition. Experiments have been successfully taken on our RoboFDM system to print general freeform objects in a support-free manner.**

I. Introduction

Additive manufacturing (AM) has been widely used in a variety of applications ranging from micro-scale fabrication of biochemical structures to large-scale construction of architecture. Although it claims the ability to fabricate shape with high complexity, the flexibility of production is still limited by the process of manufacturing. Specifically, supporting structure is needed to prevent collapse during fabrication on the regions with overhang. Drawbacks of adding supporting structures during fabrication have been extensively studied in prior research (e.g., [1], [2]).

A. Motivation

In all commercial 3D printing systems, materials are accumulated along a fix direction (i.e., the direction of gravity). The relative motion between a working platform and an extruder is always in the form of translation. The motivation of this work is to provide three additional *degrees-of-freedom* (DOF) so that the direction of material accumulation can be changed during the fabrication. Our system uses a robotic arm to provide 6-DOF motion on the printing platform. As a result, models can be fabricated in a support-free manner (see Fig.1 for an example). To prevent the bad adhesive quality of materials accumulated by a rotational extruder (e.g., the one used in [3]), the extruder is fixed in our system so that the speed of material accumulation can be well controlled with the help of gravity. This means that the function of accumulating materials along different directions is realized by moving the working platform in an inverse way. Figure 2 shows the process of fabricating a freeform model by using our system. Note that, although FDM-based 3D printing is practiced in our implementation, this method can also be applied to other types of AM.

Fig. 1. A bunny model fabricated by our RoboFDM (left) vs. the model made by conventional FDM (right). Note that, to illustrate our decomposition algorithm, different parts of the bunny model being printed along different directions are fabricated by filaments in different colors.

Besides of hardware system, the most challenging issue is how to efficiently and effectively generate a sequence of material accumulation for a given model. Although more DOFs have been gained after introducing robotic arm into the system, constraint of manufacturability still exists – i.e., the accessibility by collision-free poses. The accessibility needs to be incorporated during the sequence planning. To capture the global shape and the topology of an input model, we develop an approach based on shape analysis to generate the sequence of 3D printing in this paper.

B. Related work

The technology of AM (also named as 3D printing) appears in the late 1980s. With the development of over 30 years, 3D printing devices especially FDM-based 3D printers are now available for most consumers. Recent research (ref. [4], [5]) states the possibility of using 3D printing technology to fabricate the new robots or some parts on a robot. However, to overcome the limitation of layer-based manufacturing, research needs to take along the directions of 1) adding more DOF into motion and 2) optimizing shape or direction of fabrication.

*C. Wu and C. Dai contributed equally to this paper.
[1]C. Wu and Y-J Liu are with the TNList, Department of Computer Science and Technology, Tsinghua University, Beijing, China.
[2]C. Dai, G. Fang and C.C.L. Wang are with the Department of Design Engineering and TU Delft Robotics Institute, Delft University of Technology, Netherlands.
†Corresponding Author: c.c.wang@tudelft.nl
This work was partially supported by the seed fund of TU Delft Robotics Institute, the Natural Science Foundation of China (61432003, 61521002, 61661130156), the National Key Research and Development Plan of China (2016YFB1001202) and the Royal Society-Newton Advanced Fellowship.

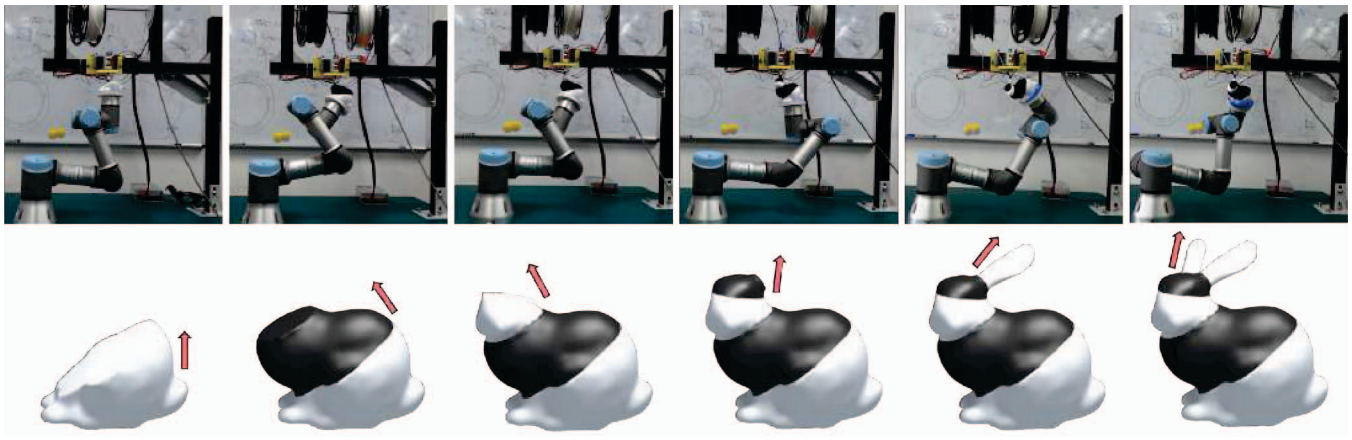

Fig. 2. The progress of using our RoboFDM system to fabricate a freeform model – bunny. Different parts of the model is fabricated along different directions (see the red arrows in illustration), and filaments in different colors are used for making different parts.

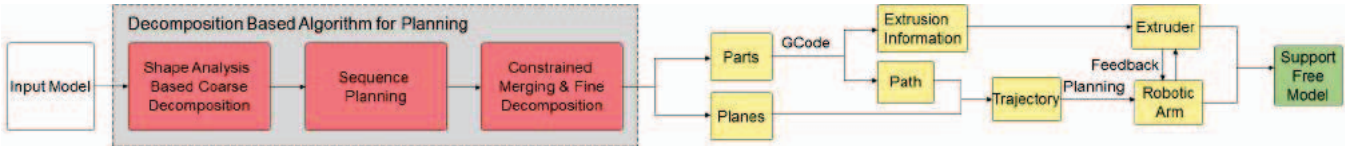

Fig. 3. Diagram to show the pipeline of our robotic system for FDM-based support-free fabrication. The major contribution of this paper is a decomposition based approach for fabrication-sequence planning and the system for realizing support-free FDM on a robot-assisted system.

More and more researchers are exploring the new DOF of 3D printing in motion so that the process of manufacturing can be improved. Keating and Oxman [6] present a manufacturing platform using 6-DOF provided by a robotic arm to fabricate models in both additive and subtractive manners, where the concept of freeform printing without supporting structures is proposed. However, only very simple shapes are fabricated in their approach and no detail of sequence and path planning is provided. Pan et al. [7] proposed a 5-axis motion system similar to 5-axis CNC machining to accumulate materials onto an existing model, where the algorithm can only deal with small components with relative simpler planning task. A 6-DOF parallel kinematic Stewart platform is presented in the work of Song et al. [8] for the purpose of multi-directional AM. Again, only small components with simple shape are processed. There is no algorithm available for fabricating general freeform models. In the recent work called RevoMaker [9], freeform models are fabricated by AM on top of an existing cubic component. The cuboidal platform used in their system cannot print general freeform models like the bunny shown in Fig.1 without supporting structures.

On the other aspect, layer-based manufacturing is still a widely used method in commercial 3D printing systems, which however needs to use additional supporting structures to avoid collapse on overhangs. A few approaches have been developed to reduce the usage of supporting structure by either model deformation or model decomposition. Hu et al. [10], [11] proposed a deformation based method to reduce 'facing down' regions. Differently, rotations are introduced in this approach during the fabrication process so that the shape of an input model does not need to be changed. Related segmentation methods are introduced in [12] and [13] to decompose an input model into pieces in the shape of height-fields. The physical model is fabricated by printing the height-field parts one by one and assembling together by glue. These segmentation methods cannot be directly applied here as collision in the process of fabrication are not considered. Our approach solves this problem by computing a collision-free decomposition.

II. System

We present a robotic solution for support-free fabrication using FDM-based material accumulation. The overview of our system is introduced below.

A. Hardware setup

The hardware setup of our system is mainly composed by a UR3 robotic arm, a FDM extruder fixed on a frame and all other control components. To demonstrate the functionality of printing multi-materials, white and black PLA filaments are used. Different regions on a model can be fabricated by using filaments in different colors. The extruder is fixed in our system, and the relative printing direction and position is realized by inverse pose of the printing platform attached on a 6-axis UR3 robotic arm. The UR3 Robotic arm is used to provide 6-DOF motion during the process of material accumulation. Considering the accuracy of positioning that can be achieved on a UR robotic [14] and the speed of fabrication, nozzles with 1mm or 2mm holes are employed in our system. Generally, 2mm nozzles are used for quick fabrication and 1mm nozzles can fabricate models with better surface quality and more geometric details.

The relative position of nozzle to the base frame of the robotic arm is also very important as it will be a problem if there are many inaccessible positions and orientations in the working envelope defined around the novel. The position to place nozzles should be optimized according to the reachability analysis of the robotic arm. First of all, we randomly sample the configurations space of UR3's joints and determine the position and orientations of each configuration point in the Euclidean space. Considering the fixed orientation of nozzle, all samples with facing-down frames are excluded. The remained frames are considered as reachable samples. The working envelope around a nozzel is defined as a bounding box $\mathcal{B}$ centered at the nozzel. The optimal position of a nozzle can then be determined by exhaustive search to find a place such that the number of frames falling in $\mathcal{B}$ is maximized.

B. Software method

The basic idea of our work is to rotate the working platform to a 'good' orientation for each segmented part so that layer-based material accumulation for this part can be completed without adding support. Specifically, a 3D model is clipped into smaller parts by planes (called *base plane* in the rest of this paper). The input model can then be fabricated following the sequence of connected parts, and the surface of each segmented part is self-supported when being printed along the normal direction of its base plane. To generate the segmentation, we propose a coarse-to-fine decomposition algorithm which first segments a model into multiple parts according to the skeleton based shape analysis (i.e., each branch a part). After that, the sequence of 'growing' is determined by incorporating the collision-free constraint of our hardware system. Finally, a fine-level partition is applied to each part to refine the sequence of printing. With the help of this decomposition algorithm, the path planning of our robotic FDM printer can be realized. For each part, layers are generated by slicing planes parallel to the part's base plane, and G-code of tool paths can be generated in the same way as conventional FDM.

The low-level software components for controlling the operation of our system are based on the ROS system. Specifically, an Arduino-based MKS Gen Board is used to control the temperature of the hot-end and also the step motor for feeding materials in each extruder. The Arduino board is set as an ROS node for communicating with UR3. In our implementation, an ROS-based driver for UR robot has been extended to add a trajectory feedback function so that operations on the robotic arm and the extruder can be synchronized.

III. Algorithms

In 3D printing, a model $\mathcal{M}$ is fabricated layer by layer along a printing direction $\mathbf{d}$. Borrowing the definitions of maximal self-support angle α_{max} and the self-supported region presented in [10], a face on $\mathcal{M}$ with its normal $\mathbf{n}$ satisfying

$$\mathbf{n} \cdot \mathbf{d} + \sin(\alpha_{max}) \geq 0 \tag{1}$$

is called *safe* face; otherwise, it is a *risky* face. A segmentation based method is developed to eliminate risky faces.

Problem Definition: Given a model $\mathcal{M}$ to be fabricated by RoboFDM, we determine a decomposition of $\mathcal{M}$ as $\{\mathcal{M}_i\}$ $(i = 1, \ldots, n)$ with

$$\mathcal{M}_1 \cup \mathcal{M}_2 \cup \cdots \cup \mathcal{M}_n = \mathcal{M}$$

so that an optimal printing direction $\mathbf{d}_i$ can be computed for each segment $\mathcal{M}_i$ to make all regions on its boundary surface $\partial\mathcal{M}_i$ safe and all components can be printed in a *collision-free* manner one by one.

A decomposition approach with three phases is developed to solve this problem, and constraints to avoid collision are incorporated into our decomposition algorithm.

A. Phase I: Shape-analysis-based coarse decomposition

In the first phase of our algorithm, a skeleton based analysis is taken to generate the first decomposition of $\mathcal{M}$ so that can decompose it into branches with each part having a simple topology (see Fig.4(a)-(d)). Specifically, the following steps are taken in our algorithm:

1) A mean-curvature flow based algorithm [15] is firstly applied to extract the 1D skeleton $\mathcal{S}_\mathcal{M}$ of $\mathcal{M}$. The number of branch, k, is determined (e.g., $k = 3$ for the bunny example shown in see Fig.4(b)).
2) For every point $\mathbf{p}$ on the surface $\partial\mathcal{M}$, a shape diameter metric $D(\mathbf{p})$ is evaluated by its distance to the closest point on $\mathcal{S}_\mathcal{M}$ (see Fig.4(c)).
3) An expectation maximization algorithm is conducted to fit k Gaussian to the histogram of $D(\cdot)$ on $\partial\mathcal{M}$ to first have a soft-clustering of faces to k clusters based on the values of their shape diameter metrics. This is followed by a hard partition of faces using k-ways graph-cut to consider local geometry on $\partial\mathcal{M}$ (Details can be found in [16]).

Note that, different from the original approach presented in [16], a 1D skeleton computed from mean-curvature flow is used here to enhance the robustness of partition. Applying one iteration of Laplacian smoothing to $\mathcal{M}$ before the above three steps cab further enhance the robustness of the algorithm.

Boundaries of surface regions obtained from above method are not planar, which are hard to be used in the layer-based AM. We generate the decomposition of $\mathcal{M}$ by fitting and adjusting the separating planes between different parts. Specifically, we first sample the boundary curve between two segmented patches into points, and their inward/outward offset points can be generated along the surface normals with a very small offset value. Principal component analysis is then applied on all these points to obtain a cutting plane approximating the boundary between two patches. These planes now form a coarse decomposition of the input model, $\mathcal{M}$.

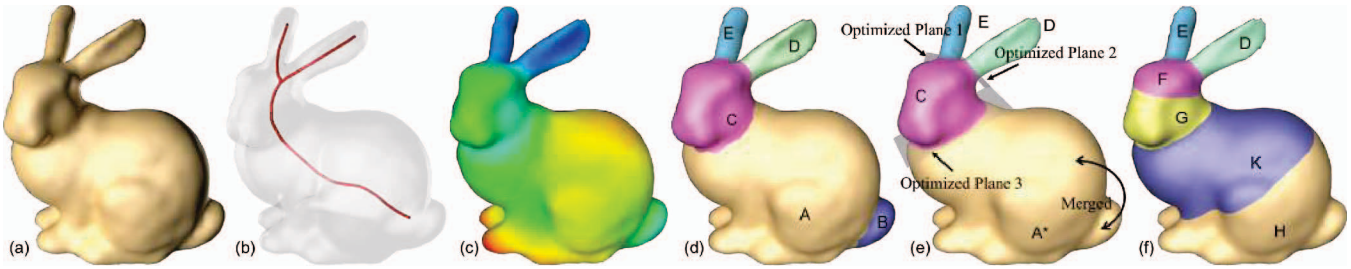

Fig. 4. Progressive results of our algorithm on the bunny model: (a) input, (b) extracted skeleton, (c) distribution of the shape diameter metric, (d) the result of coarse segmentation, (e) the result after plane perturbation and merging, and (f) the final result after fine decomposition.

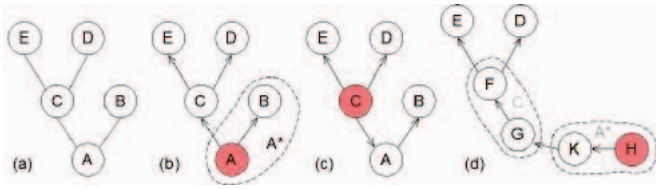

Fig. 5. The graph representation of the bunny model for sequence planning: (a) an undirected graph as the result of coarse decomposition, (b) a directed graph if the sequence start from node 'A', (c) another possible directed graph with node 'C' as the root, and (d) the resultant graph after applying the merging and fine decomposition steps in Phase III of our algorithm. 'A' and 'B' are merged into a new node 'A*', which is further split into 'K' and 'H' in the fine decomposition step. The nodes 'F' and 'G' in (d) are split from 'C'. Corresponding region of each node can be found in Fig.4.

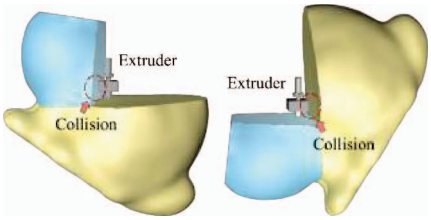

Fig. 6. Collision between the nozzle and the printed model occurs when the base cross-sections intersect with each other – changing the sequence of fabrication cannot resolve the problem.

B. Phase II: Sequence planning

To build the sequence of printing, the result of a coarse decomposition can be first converted into an undirected graph $\mathcal{G}$ by using the neighboring information between parts. Specifically, each part $\mathcal{M}_i$ is considered as a node in $\mathcal{G}$. When $\mathcal{M}_i$ and $\mathcal{M}_j$ are connected, an undirected edge is constructed in $\mathcal{G}$ to represent this neighborship. For example the bunny model shown in Fig.4, its undirected graph can be defined as shown in Fig.5(a). Starting from a selected node (e.g., node 'A' in Fig.5(b)), we can generate a sequence of nodes on the graph by a breadth-first-traversal. The order of visit gives the directions of edges – i.e., $\mathcal{G}$ is converted into a directed graph $\bar{\mathcal{G}}$ with the starting node named as *root*. Note that, this conversion depends on the starting node of search. When starting from a different node, a different graph can be generated (e.g., the directed graph with node 'C' as a root is shown in Fig.5(c)). In our current implementation, the root is interactively selected by users.

After getting the sequence of printing based on the coarse decomposition, the orientation of printing can be determined according to the planes separating different parts of $\mathcal{M}$. When two parts $\mathcal{M}_i$ and $\mathcal{M}_j$ are separated by a plane $P_{i,j}$ and have the printing sequence of $\mathcal{M}_i$ followed by $\mathcal{M}_j$, the process to fabricate $\mathcal{M}_j$ will start from accumulating materials on the plane $P_{i,j}$. Defining the normal $\mathbf{n}_{i,j}$ of $P_{i,j}$ in an orientation pointing from $\mathcal{M}_i$ to $\mathcal{M}_j$ (with $\mathbf{n}_{j,i}$ having an inverse orientation), the printing direction of $\mathcal{M}_j$ is heuristically given as $\mathbf{n}_{i,j}$. Taking this heuristic to determine the printing direction of each component, we need to further adjust the separating planes in the last phase of our algorithm.

The oriented plane $P_{i,j}$ is named as the *base plane* for the fabrication of $\mathcal{M}_j$, and the cross-section $P_{i,j} \cap \mathcal{M}$ is called the *base cross-section*. Besides, the printing direction of root $\mathcal{M}_r$ is determined by finding an optimal one resulting in a minimal facing down area while keeping all separating planes at the boundary of $\mathcal{M}_r$ facing up.

C. Phase III: Constrained fine tuning

With the printing direction determined from the base cross-section of a part $\mathcal{M}_i$, the risky region of $\mathcal{M}_i$ can be defined as the surface regions on $\partial\mathcal{M}_i$ (excluding the base plane) that do not satisfy Eq.(1). The area of risky region, $R(\cdot)$, is a metric used in our constrained fine tuning. A completely support-free component $\mathcal{M}_i$ should have $R(\mathcal{M}_i) = 0$. The constraints to prevent collision are:

- *Constraint I* – The cross-sections formed by the separating planes (i.e., the base cross-sections) should not intersect with each other (as illustrated in Fig.6).
- *Constraint II* – All base planes need to face up.

In this phase of our algorithm, the decomposition is further refined by applying 1) plane perturbation, 2) region merging and 3) fine decomposition. Each part of the decomposed model will be ensured to be support-free, and the heuristic constraints for avoiding collision will be incorporated.

Plane Perturbation The separating planes determined by PCA in the phase of coarse decomposition will be further optimized to enhance the manufacturability of each part. For a plane $P_{i,j}$ separating $\mathcal{M}_i$ and $\mathcal{M}_j$, small random perturbation is added to its position (with offset less than 2.5% of the bounding-box's diagonal length) and orientation (within 5° angular variation). The areas of cross-sections formed by the perturbed planes are computed, and those

lead to more than 20% area increase in cross-section will be excluded. The total area of risky regions on $\mathcal{M}_i$ and $\mathcal{M}_j$ is evaluated as $R(\mathcal{M}_i) + R(\mathcal{M}_j)$. A separating plane leads to the smallest value is considered as optimum to be used.

Region Merging As the coarse decomposition based on shape analysis did not explicitly consider the area of risky region (i.e., manufacturability), it is possible that a component merged from two neighboring parts has smaller risky region. The parts 'A' and 'B' of the bunny example shown in Fig.4 are a good example – merged into a new part 'A*' (see also the graph representation in Fig.5). Base plane that is visited earlier in the determined printing sequence will be used as the new base plane. For example on the bunny model, the base plane of 'A' will be used as the base plane of 'A*'.

Fine Decomposition Nodes on the directed graph representing the decomposition will be further refined to ensure the manufacturability. A greedy strategy is applied here. The component with largest risky area, $\mathcal{M}_g$, is selected to be clipped into two components, $\mathcal{M}_g^s$ and $\mathcal{M}_g^t$, by an optimal plane that can minimize the total area of risky region and satisfy the constraints for preventing collision. After applying this refinement, the node $\mathcal{M}_g$ on the direct graph and in the sequence of printing will be replaced by $\mathcal{M}_g^s$ and $\mathcal{M}_g^t$. The refinement on most risky region is repeatedly applied until all components become safe (see the result in Fig.4 and Fig.5(d) as an example). In our implementation, we select k regions from the top of queue ($k = 6$) instead of only the most risky one to avoid being stuck at the local minimum during the refinement.

Optimal Cutting Plane All possible planes $\pi_{k,l} = (\mathbf{n}_k, d_l)$ with planar equation $\mathbf{n}_k \cdot \mathbf{x} - d_l = 0$ that satisfy constraints I and II are considered. The upper half of Gaussian sphere is uniformly sampled into 100 points for the possible values of $\mathbf{n}_k$, and the plane offsets $\{d_l\}$ are also sampled uniformly at intervals of 5mm in our implementation. This follows the same sampling strategy of clipping planes in Chopper [17]. Among all these planes, the optimal plane for clipping is defined as

$$\arg\max_{\pi_{k,l}} (R(\mathcal{M}_g) - (R(\mathcal{M}_g^s) + R(\mathcal{M}_g^t))) \qquad (2)$$

with $\mathcal{M}_g^s$ and $\mathcal{M}_g^t$ being the two sub-parts clipped from $\mathcal{M}_g$ by $\pi_{k,l}$ (i.e., $\mathcal{M}_g^s \cup \mathcal{M}_g^t = \mathcal{M}_g$ and $\mathcal{M}_g^s \cap \mathcal{M}_g^t = \pi_{k,l}$).

IV. Implementation Details and Results

The decomposition based planning algorithm presented above has been implemented in a C++ program to generate mesh models for each component. The slicing software for conventional FDM is used to generate planar slices and tool paths according to the printing directions determined in our algorithm. G-code for AM can be generated from the planned paths and sent to the motion-control module of our system.

The motion of UR3 is realized by first determining the pose of its end-effector according to a given position and orientation for material accumulation in the Euclidean space.

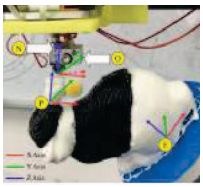

Fig. 7. Frames used in the motion control of our RoboFDM system.

Fig. 8. More examples that are fabricated by our RoboFDM system – (left) Armadillo and (right) Hanging-Ball without adding any supporting structure.

As illustrated in Fig.7, there are five different frames in our system including:

- *B*: Frame of the base link on the robotic arm, which is also set as the origin of world-coordinate system;
- *E*: Frame of the end-effector with origin located at the center of the first base plane to print;
- *P*: Frame for the current part to be printed with origin located at the center of the current base plane for printing;
- *O*: Frame at the current position and orientation to accumulate material;
- *N*: Frame of the FDM extruder with origin at the end of nozzle.

The relationship among these frames can be defined as

$$\mathbf{T}_E^B \mathbf{T}_P^E \mathbf{T}_O^P = \mathbf{T}_N^B, \qquad (3)$$

where $\mathbf{T}_N^B$ is a constant matrix as the extruder is fixed in our system, $\mathbf{T}_O^P$ is known according to the tool-path represented by G-code, and $\mathbf{T}_P^E$ can be updated during the printing process. With these known transformations, $\mathbf{T}_E^B$ can be obtained by solving Eq.(3). After determining $\mathbf{T}_E^B$, inverse kinematics is applied to compute a corresponding configuration in the joint space of UR3. The motion between poses is generated by using the *RRT-Connect* based planning [18], with which collision can be avoided.

We have tested our system by printing a variety of models in a support-free manner. Figure 3 has shown the whole process of printing a support-free bunny model, where supporting structures must be added below the head and at the ears by using conventional 3D printing (see the right of Fig.1). Figure 8 shows our results of decomposition and fabrication on two other models. Statistic of computation and fabrication is given in Table I.

At the same time, we also test the mechanical properties of a model fabricated by RoboFDM and compare it with the same model fabricated by conventional 3D printing. As shown in Fig.9, the stiffness of model fabricated by RoboFDM is weaker, which is mainly caused by the weak adhesion of materials at the interface between two regions.

TABLE I
STATISTIC OF FABRICATION

Model	Bunny	Armadillo	Hanging-Ball
Number of Facets	10,000	17,142	5,984
Decomposition Time	171 sec.	269 sec.	156 sec.
Fabrication Time	152 min.	263 min.	85 min.

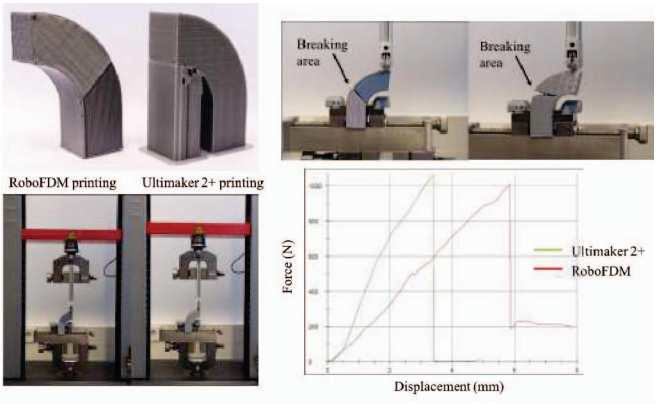

Fig. 9. Mechanical tests taken on models fabricated by RoboFDM and conventional 3D printing.

On the other aspect, the delamination of layers happens at nearly the same level of loading (i.e., around 1000N).

V. CONCLUSION AND DISCUSSION

We propose a novel robotic system to fabricate models in support-free 3D printing. The 6-DOF motion is provided to the working platform so that materials can be accumulated along different directions in the working space with a fix extruder. The core part of our system is a model decomposition algorithm, which segments an input model into parts that can be printed without adding supporting structures. The sequence of printing is determined together with the decomposition. Our experimental tests give promising results, and the models with large overhangs can be fabricated in a support-free way.

There are still some limitations in our current implementation of RoboFDM, which fall into the following aspects.

1) *Speed*: We set the motion of robotic arm at a very slow speed to ensure the accuracy of positioning; therefore, the fabrication time in own system is longer than the conventional FDM printer for the same model. A better method for accurate positioning needs to be developed.

2) *Size*: As the nozzle is fixed in our current setup, the volume of a model to be printed is quite limited by the frames and the table. This can be improved when we add two more DOF to the frame and the nozzle in motion.

3) *Cost of System*: The hardware cost of using a robot arm to fabricate models is much higher than using a conventional 3D printer. On the other aspect, more flexibility of fabrication is given by the RoboFDM system.

4) *More complex shape*: Our decomposition algorithm may fail on models with high genus number, on which supporting structures still need to be added for printing.

5) *Better strategy of collision-free*: The constraint to avoid facing down base planes employed in this paper is too restrict although it works well for preventing collision. As a result, the support free printing of some model (e.g., a tree with pointing down branches) may fail. We plan to work out better constraints for collision avoidance.

In summary, although this work of robot-assisted additive manufacturing gives promising results in experiments, there are still a few challenges to be tackled in our future research.

REFERENCES

[1] W. Gao, Y. Zhang, D. Ramanujan, K. Ramani, Y. Chen, C. B. Williams, C. C. Wang, Y. C. Shin, S. Zhang, and P. D. Zavattieri, "The status, challenges, and future of additive manufacturing in engineering," *Computer-Aided Design*, vol. 69, pp. 65–89, 2015.

[2] X. Zhang, X. Le, A. Panotopoulou, E. Whiting, and C. C. L. Wang, "Perceptual models of preference in 3d printing direction," *ACM Trans. Graph.*, vol. 34, no. 6, pp. 215:1–215:12, Oct. 2015.

[3] S. Mueller, S. Im, S. Gurevich, A. Teibrich, L. Pfisterer, F. Guimbretière, and P. Baudisch, "Wireprint: 3D printed previews for fast prototyping," in *Proceedings of the 27th Annual ACM Symposium on User Interface Software and Technology*, 2014, pp. 273–280.

[4] D. Rus and M. T. Tolley, "Design, fabrication and control of soft robots," *Nature*, vol. 521, pp. 467–475, 2015.

[5] N. Bezzo, A. Mehta, C. D. Onal, and M. T. Tolley, "Robot makers: The future of digital rapid design and fabrication of robots," *IEEE Robotics Automation Magazine*, vol. 22, no. 4, pp. 27–36, 2015.

[6] S. Keating and N. Oxman, "Compound fabrication: A multi-functional robotic platform for digital design and fabrication," *Robotics and Computer-Integrated Manufacturing*, vol. 29, no. 6, pp. 439–448, 2013.

[7] Y. Pan, C. Zhou, Y. Chen, and J. Partanen, "Multitool and multi-axis computer numerically controlled accumulation for fabricating conformal features on curved surfaces," *ASME Journal of Manufacturing Science and Engineering*, vol. 136, no. 3, 2014.

[8] X. Song, Y. Pan, and Y. Chen, "Development of a low-cost parallel kinematic machine for multidirectional additive manufacturing," *ASME Journal of Manufacturing Science and Engineering*, vol. 137, no. 2, 2015.

[9] W. Gao, Y. Zhang, D. C. Nazzetta, K. Ramani, and R. J. Cipra, "RevoMaker: Enabling multi-directional and functionally-embedded 3d printing using a rotational cuboidal platform," in *Proceedings of the 28th Annual ACM Symposium on User Interface Software and Technology*, 2015, pp. 437–446.

[10] K. Hu, S. Jin, and C. C. L. Wang, "Support slimming for single material based additive manufacturing," *Computer-Aided Design*, vol. 65, pp. 1–10, 2015.

[11] K. Hu, X. Zhang, and C. C. L. Wang, "Direct computation of minimal rotation for support slimming," in *2015 IEEE International Conference on Automation Science and Engineering (CASE)*, 2015, pp. 936–941.

[12] P. Herholz, W. Matusik, and M. Alexa, "Approximating free-form geometry with height fields for manufacturing," *Computer Graphics Forum*, vol. 34, no. 2, pp. 239–251, 2015.

[13] R. Hu, H. Li, H. Zhang, and D. Cohen-Or, "Approximate pyramidal shape decomposition," *ACM Trans. Graph.*, vol. 33, no. 6, pp. 213:1–213:12, 2014.

[14] C.J.Kruit, "A novel additive manufacturing approach using a multiple degrees of freedom robotic arm," Master's thesis, Delft University of Technology, August 2013.

[15] A. Tagliasacchi, I. Alhashim, M. Olson, and H. Zhang, "Mean curvature skeletons," *Computer Graphics Forum*, vol. 31, no. 5, pp. 1735–1744, 2012.

[16] L. Shapira, A. Shamir, and D. Cohen-Or, "Consistent mesh partitioning and skeletonisation using the shape diameter function," *Visual Computer*, vol. 24, no. 4, pp. 249–259, 2008.

[17] L. Luo, I. Baran, S. Rusinkiewicz, and W. Matusik, "Chopper: Partitioning models into 3d-printable parts," *ACM Trans. Graph.*, vol. 31, no. 6, pp. 129:1–129:9, 2012.

[18] J. J. Kuffner and S. M. Lavalle, "RRT-connect: An efficient approach to single-query path planning," in *Proc. IEEE Intl Conf. on Robotics and Automation*, 2000, pp. 995–1001.